Chemical Engineering Journal 340 (2018) 66–72

Contents lists available at ScienceDirect

Chemical Engineering Journal

journal homepage: www.elsevier.com/locate/cej

Single phase microreactor for the continuous, high-temperature synthesis of < 4 nm superparamagnetic iron oxide nanoparticles

Laura Uson[a,b], Manuel Arruebo[a,b,*], Victor Sebastian[a,b,*], Jesús Santamaria[a,b]

[a] Institute of Nanoscience of Aragon (INA) and Department of Chemical, Engineering and Environmental Technology, University of Zaragoza, C/ Mariano Esquillor, s/n, I+D+i Building, 50018 Zaragoza, Spain

[b] CIBER de Bioingeniería, Biomateriales y Nanomedicina (CIBER-BBN), Centro de Investigación Biomédica en Red, C/ Monforte de Lemos 3-5, Pabellón 11, 28029 Madrid, Spain

GRAPHICAL ABSTRACT

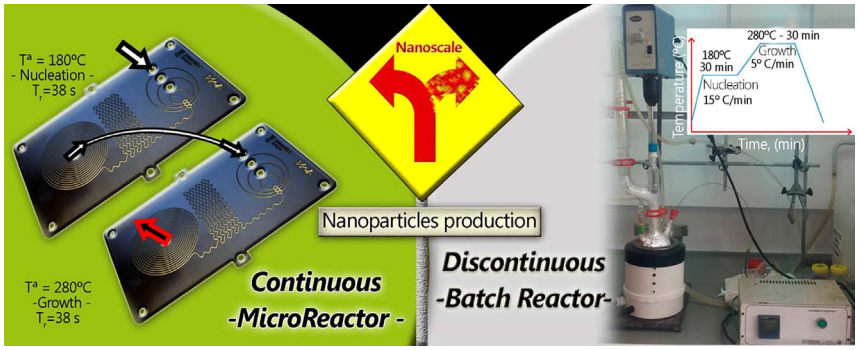

ARTICLE INFO

Keywords:
Microchannel emulsification
Hybrid nanomaterials
Microfluidics
Bio-nanomaterials
Continuous production

ABSTRACT

The reproducibility of key nanomaterial features is essential in nanomedicine applications where small changes of physical characteristics often lead to a very different behavior. In this regard, continuous microreactors are often advocated as a means to achieve highly precise synthesis of nanomaterials. However, when the synthesis must take place at high temperatures the use of these devices becomes restricted in terms of materials and practical problems (e.g. plugging of microchannels). Here we present the continuous synthesis of ultrasmall superparamagnetic iron oxide nanoparticles (SPIONs) through a polyol-based process at high temperatures (> 200 °C). The microfluidic reactor designed allows SPION production at residence times under 1 min, was able to work continuously for 8 h without channel blockage and reached high production yields by coupling microreactors using stacked plates. The effect of operating conditions was optimized to produce homogeneous particles with a narrow particle size distribution. In summary, the microreactor developed in this work enables easy-to scale up, reproducible continuous production of SPIONs.

1. Introduction

Superparamagnetic iron oxide nanoparticles (SPIONs) have been advocated for a plethora of biomedical applications [1,2] such as cellular therapy, tissue repair, drug delivery, magnetic resonance imaging (MRI), *in vivo* cell tracking, hyperthermia, bioseparation and

* Corresponding authors at: Institute of Nanoscience of Aragon (INA) and Department of Chemical, Engineering and Environmental Technology, University of Zaragoza, C/ Mariano Esquillor, s/n, I+D+i Building, 50018 Zaragoza, Spain.
E-mail addresses: arruebom@unizar.es (M. Arruebo), victorse@unizar.es (V. Sebastian).

https://doi.org/10.1016/j.cej.2017.12.024

Available online 11 December 2017

magnetofection, just to name a few. In these biological applications, SPIONs must combine properties of high magnetic moment and biocompatibility. Superparamagnetism implies that under the presence of a magnetic field magnetic NPs have zero magnetization at a zero applied field, and no remnant magnetism or coercive field are exhibited when the magnetic field is removed. The magnetic properties depend strongly on the NP crystallinity and size. As the particle size decreases, a multidomain ferromagnetic material can become single-domain when the thermal energy is enough to overcome the anisotropy energy, and the material, in that situation presents superparamagnetic behavior. This occurs at a critical size that is characteristic of each material. For instance, in the case of iron oxides, an intermediate superparamagnetic–ferromagnetic transition region in the range of 10–13 nm is observed, having ferromagnetic behavior at particle sizes above 13 nm [3]. SPIONs have been produced by different routes, ranging from gas to liquid phase: coprecipitation, thermal decomposition, hydrothermal or solvothermal synthesis, sol-gel, microemulsion, sonochemical, electrochemical and laser ablation [4]. Of these routes, the thermal decomposition of metallic precursors provides SPIONs with excellent crystallinity and precise control of particle sizes [5]. Thermal decomposition of metallic precursors is frequently carried out in hot organic high boiling-point solvents with ligands that tune the particle size/shape. However, the use of toxic solvents and ligands often decreases the biocompatibility of the final product. In addition, SPIONs should be water dispersible, and therefore the use of hydrophilic ligands is preferred. The polyol process fulfills aforementioned requirements and has been widely used in the production of SPIONs due to the demonstrated advantages of glycol [6]: 1) high-boiling solvent with low toxicity; 2) reducing agent, 3) stabilizer and 4) enables the kinetic control of experimental conditions. Cai et al. [6] reported a polyol-synthesis procedure for the synthesis of homogenous SPIONs by heating the reagents at a fast heating rate (15 °C/min). This procedure consisted in two consecutive stages: 1) Nucleation, at 180 °C during 30 min. and 2) Growth, at 280 °C for another 30 min. Although the synthesis procedure is not complex, an excellent control of reaction conditions is required. This fine control enables to direct the formation of intermediate complexes to tune the nucleation stage and then, the resulting particle-size distribution shows high monodispersity. Certainly, this procedure was thoroughly studied by the controlled modification of its main synthesis parameters [7,8]: heating rate, aging time, reflux time, solvents and reagent concentrations.

Since the efficient application of SPIONs is highly sensitive to their mean particle size and to the width of their particle size distribution, there is a strong need for new synthetic methods that are capable of yielding high quality SPIONs. In addition, this type of NPs is prone to agglomeration and oxidation (i.e., from magnetite to maghemite) upon long-term storage, and therefore synthesis procedures that enable automated local on-demand production become attractive. Conventional batch reactors are still frequently employed to prepare NPs at both lab-scale and large production in spite of their serious limitations to deliver nanomaterials with a tight control of their properties at the nanoscale [9]. These limitations are originated by their inefficient heat and mass transfer rates, leading to significant variations of local conditions within the reactor. The lack of control in reaction parameters becomes even more critical in fast kinetic reactions, where the reaction time can be comparable to the mixing time [10]. A non-homogeneous mixing of reagents or significant variations in local temperatures will produce difference particle nucleation and growth rates throughout the reactor, yielding a heterogeneous formation of NPs.

Microfluidic reactors are considered as an alternative technology to enable excellent control on the synthesis parameters during NP crystallization [11,12]. Continuous flow microreactors integrate heaters and fluid control elements that offer a solution to the shortcomings produced in batch-type reactors [13]. Microreactors present inherent advantages, including enhancement of mass and heat transfers, feedback control of temperature and feed streams, good synthesis reproducibility, and low reagent consumption during optimization [11]. In addition, the problems posed by fast kinetically-controlled reactions can be overcome thanks to: 1) the small reaction volumes involved, 2) the high surface to volume ratio of microchannels and 3) the high heat and mass transfer rates. Seminal work in polymer-based [14–18], and glass-based microreactors [19], has clearly shown the benefits of using microfluidic reactors to produce magnetic nanoparticles. However, these synthesis procedures were carried out at low temperatures (< 90 °C) following the co-precipitation method. Considering that crystallinity and then, magnetization, are improved by a higher synthesis temperature [7] and that co-precipitation is not as precise in terms of size control as the thermal decomposition technique, the aim of this work is the development of an scalable and reproducible procedure capable to produce SPIONs continuously at high temperatures (> 200 °C) using the thermal decomposition polyol-based process. To this end, we have designed a microfluidic platform based on micropatterned plates to achieve excellent control in the continuous production of SPIONs from the thermal decomposition of Fe iron(III) acetylacetonate [$Fe(acac)_3$].

2. Experimental section

2.1. Materials

Iron(III) acetylacetonate [$Fe(acac)_3$] (≥97%, Sigma-Aldrich), triethylene glycol (TEG, 99%, Sigma-Aldrich), absolute ethanol, ethyl acetate (ACS reagent, ≥99.5%, Sigma-Aldrich), hydrochloric acid (HCl, 36.5%, Sigma-Aldrich) were used without further purification.

2.2. Microfluidic system and continuous synthesis procedure

The experimental system consists of two consecutive stainless steel microreactors. The first microreactor was heated at 180 °C, while the second one was heated at 280 °C. This configuration is intended to emulate the batch-synthesis procedure reported by Cai et al. [6], where the batch reactor was sequentially heated at 180 °C and 280 °C for 30 min in each heating stage. The microreactor plates were similar to those used by Jensen et al. [20,21] based on metal plates, but the design was adapted for the specific needs of this process, as described below. The microreactor consists of a stainless steel (AISI 316) plate (88 mm × 50 mm × 0.5 mm) patterned with two different zones (Fig. 1-a, b): 1) Mixing zone, using a meandering microchannel to promote a fast passive mixing [22] and 2) Reaction zone, a spiral microchannel that minimizes the fouling process during particle growth [22]. The plates were fabricated using a chemical etching procedure developed by Exella (Exella Europe SRL—www.exella.es), (Fig. 1-b). The microchannels were 370 µm wide, with a depth of 150 µm being the reactor volume of 160 µL.

The plate had three fluid inlet ports and one outlet port. The plate was compressed in an aluminum block and contacted with high-temperature resistant polymeric gaskets (TEADIT® NA1122), (Fig. 1-f). The plates were assembled with different configurations to optimize the nanocrystallization reaction and to control the particle size distribution: 1) Individual (Fig. 1-d), 2) In series to separate the nucleation and growth stages (Fig. 1-c) and 3) Stacking several plates to increase the microreactor volume and to increase the SPIONs productivity (Fig. 1-e). There were two options to assemble the stacked plates: 1) In parallel by splitting the inlet flow and 2) In series, where the inlet flow is not split. Both options obey the same value of t_m (residence time, Eq. (1)), but we selected the assembled of plates in series to increase the linear velocity and to prevent microchannel blockage.

$$t_m = \frac{Number\ of\ plates\ \times Volume_{Plate}}{Total\ Flow} \quad (1)$$

The aluminum block was equipped with four heating cartridges to assure a homogenous heating and thermocouples were included to

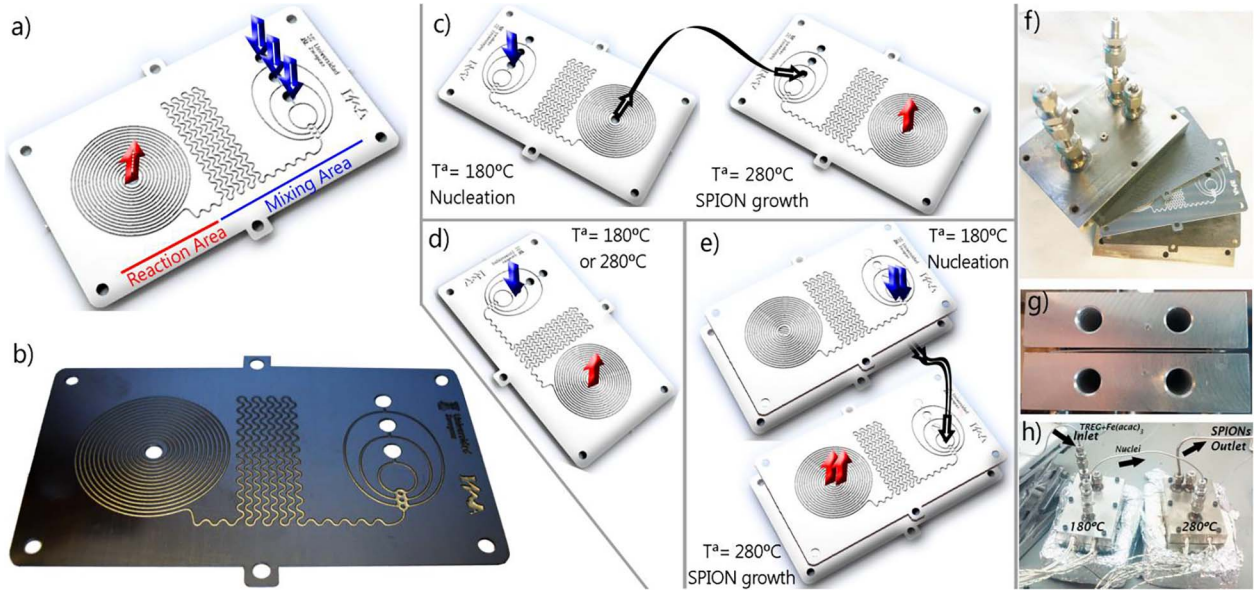

Fig. 1. a) Scheme of the micropatterned plate and the location of the mixing and reaction zones; b) Stainless-steel micropatterned plate used in this work; A variety of configurations to assemble the micropatterned plates: c) Plates assembled in series to achieve independent control of nucleation and growth stages, d) Single plate where nucleation and growth take place simultaneously and e) Assembly of stacked plates in series to increase the microreactor volume and the productivity; f) Assembly of the microreactor: heating block, polymer gaskets and micropatterned plate; g) Heating cartridges housings in the heating block; h) Microfluidic system consisting of two microreactors assembled in series to operate at 180 °C and 280 °C, respectively.

control the setup temperature (Fig. 1 g, h). A 9.4 mM of $Fe(acac)_3$ in TEG solution was loaded in high-pressure stainless steel syringes (Harvard Apparatus) and introduced by means of syringe pumps (Harvard Apparatus PHD Ultra™ CP 4400), ensuring a good control of the flow rates with very low pulsation. The syringes and heating blocks were connected to 1/16″ stainless-steel tubing. Following SPIONs synthesis by thermal decomposition, the nanoparticles were purified by adding a mixture of ethyl acetate and ethanol (2:1) to the SPIONs with a 5:1 v/v (washing mixture: SPIONs) and then centrifuged at 8000 rpm for 10 min to yield a black solid and supernatant containing unused reactants.

2.3. SPIONs characterization

Transmission electron microscopy observations were carried using a T20-FEI microscope with a LaB6 electron source fitted with a "SuperTwin®" objective lens allowing a point-to-point resolution of 2.4 Å. A 10μL suspension of purified SPIONs was pipetted onto a TEM copper grid having a continuous carbon film. Samples were let to evaporate completely and then analyzed. Aberration corrected scanning transmission electron microscopy (Cs-corrected STEM) images were acquired at LMA-INA-UNIZAR using a high angle annular dark field detector in a FEI XFEG TITAN electron microscope operated at 300 kV equipped with a CETCOR Cs-probe corrector from CEOS Company allowing formation of an electron probe of 0.08 nm.

The yield of the reaction was studied by UV–VIS spectroscopy (V-670 Jasco Co.) analyzing the 350 nm band corresponding to acetylacetonate [7].

Magnetic behavior of the samples was studied, at 37 °C (considering potential physiological applications), in a Superconducting Quantum Interference Device magnetometer (SQUID) from Quantum Design's, model MPMS-XL.

The analysis of the magnetic phase, crystalline properties and purity was studied by X-ray diffraction. The analyses were carried out using a Philips X-Pert diffractometer equipped with a monochromatized Cu-Kα radiation (40 kV, 20 mA) from 25 to 80° with a step size of 0.013°.

3. Results and discussion

Fig. 1 illustrates the microfluidic reactor designed to produce SPIONs by the thermal decomposition of iron(III) acetylacetonate at high temperatures. Metal-based microreactors are especially advantageous for processes involving high temperatures with a requirement of fast heat transfer to reduce temperature inhomogeneity. In addition, the mechanical strength, low cost and easy replacement of stainless steel plates, are useful properties for the production of nanomaterials at high temperature conditions (> 200 °C). In a previous work, the successful production of indium phosphide nanocrystals at high temperature (320 °C) was achieved in a multi-stage silicon-based microfluidic system, where the nucleation and growth were separated to gain control of NPs characteristics [23]. SPIONs have been produced in this work using the same nanocrystallization strategy, using the knowledge gained on the growth mechanism and the effect of synthesis variables gained in batch reactor studies [6–8], especially the effect of temperature in the nucleation and growth stages and the type of solvent used. Although the direct translation of a batch process into a microfluidic process is not trivial and a proper initial screening of synthesis conditions is required, it was assumed in this work that the SPION nucleation was a thermodynamically driven process. This fact implies that the reaction temperature in the nucleation stage should be similar to the one obtained in previous studies in batch-type reactors [6,7]. On the other hand, it is well known that the crystallinity and magnetization of SPIONs, as well as the growth kinetics are enhanced as the synthesis temperature increases. Then, considering the thermal stability of the polymeric gaskets, a temperature of 280 °C was selected as the appropriate growth temperature to enable a fast production of high quality SPIONs. The following sections describe the most important achievements obtained in this work to optimize the continuous production of SPIONs at high temperatures by thermal decomposition of iron(III) acetylacetonate.

3.1. Effect of residence time

It is well-known that one of the benefits of using microfluidic systems to produce nanomaterials is that the synthesis time is often

Residence Time*/reactor	Flow rate, µL/min	Observations
9.6 s	1000	Good performance
12.8 s	750	Good performance
19.2 s	500	Good performance
27.4 s	350	Good performance
38.4 s	250	Blockage

* Residence time in nucleation and growth microreactors

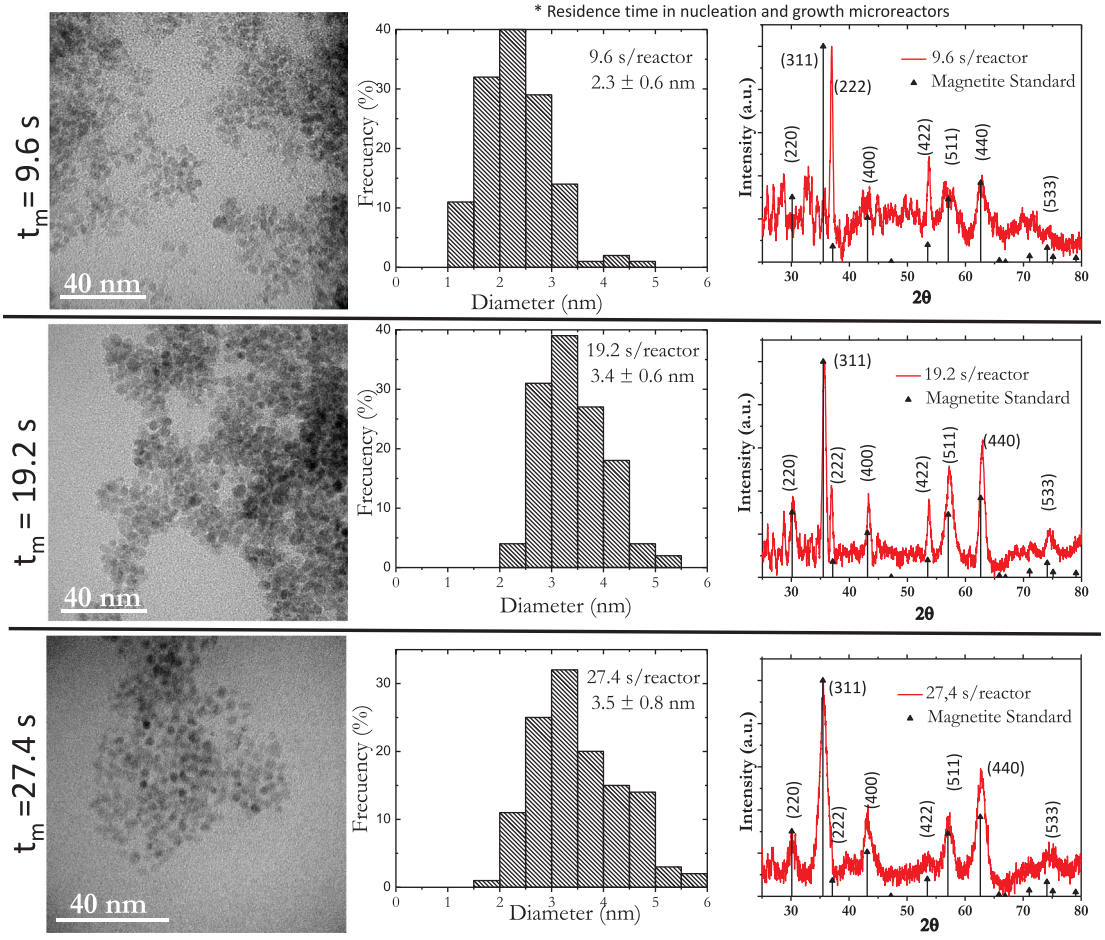

Fig. 2. Production of SPIONs with two microreactors (1 plate/microreactor) assembled in series: 1) Nucleation at 180 °C and 2) Growth at 280 °C. Experimental details and characterization data at different t_m values: 9.6 s, 19.2 s and 27.4 s. Particle size histograms were plotted after measuring at least 150 particles per sample. Magnetite Standard (Joint Committee on Powder Diffraction Standards – JCPDS card number 89-0691).

reduced due to the fast heat and mass transfers [13]. In our case the objective for the production of SPIONs was to lower the reaction times to minutes, rather than the timescale of hours required in batch type reactors [6,7]. However, the blockage of microchannels can be a major concern. This phenomenon is caused either by NP agglomeration and sedimentation at the low linear rates usually employed in microreactors, or by a preferential heterogeneous nucleation in the wall surfaces of microchannels. To study this problem two single-plate microreactors were assembled in series to better control the nucleation and growth stages (Figs. 1-c and 2): 1) Nucleation microreactor and 2) Growth microreactor. We found that if the t_m value of the microreactor in which growth takes place were larger than 27.4 s, the SPIONs production was not stable and the microfluidic system blocked after a time lapse of several minutes. The main microchannel fouling was occurring at the curved channel sections, where the slow flow rates (< 300 µL/min) and low linear velocities promote the sedimentation of aggregates that eventually block the microchannel. To circumvent this problem t_m was decreased by increasing the reagent flow rates. Fig. 2 illustrates the SPIONs produced at different t_m values: 9.6 s, 19.2 s and 27.4 s. A black and stable colloid was obtained in all tested conditions, assuring the SPIONs production for 8 h without blockage. The black color was indicative that no Fe^{3+} oxo-hydroxides were formed [18].

TEM analysis of representative SPIONs synthesized under different t_m revealed that isotropic NPs were produced with a lognormal size distribution of mean particle size smaller than 4 nm. The data showed that doubling t_m from 9.6 s to 19.2 s produced larger SPIONs (3.4 ± 0.6 nm vs. 2.3 ± 0.6 nm). However, an additional increase of residence time to t_m = 27.4 s did not cause a further modification of the SPIONs size (3.5 ± 0.8 nm), the slight variation on the particle size observed is not statistically significant. Interestingly, XRD diffraction analysis revealed that all tested conditions yielded pure magnetite nanocrystals. This is an excellent achievement because it is common to have a mixture of iron oxide phases when the batch reaction is translated to a microreactor process [15,19]. The broad peaks of XRD spectra are in agreement with the small crystallite size of the SPIONs produced. The crystalline structure is sensitive to t_m, SPIONs produced with a t_m = 9.6 s have a greater tendency to promote the growth of (2 2 2) planes, whereas a long residence time (19.2 s or 27.4 s) promoted the preferential growth of (3 1 1) and (4 4 0) planes. The low signal-to-noise ratio of XRD spectra collected form SPIONs produced at t_m = 9.6

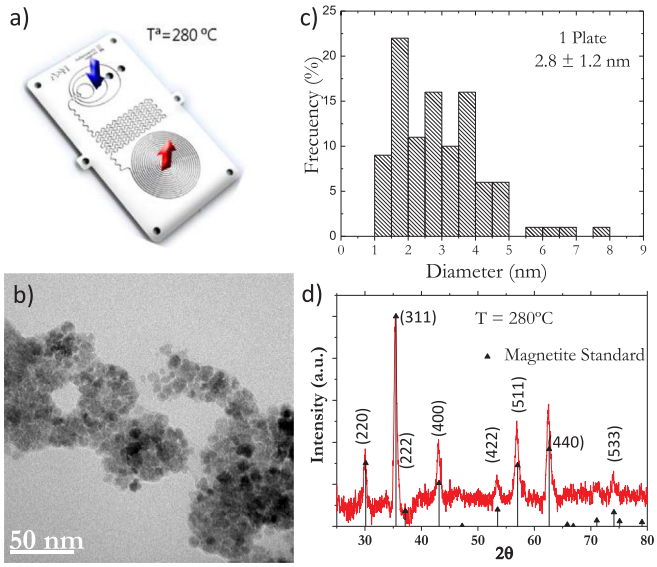

Fig. 3. Production of SPIONs with a single microreactor with one plate at 280 °C and t_m = 27.4: a) Scheme of stream distribution; b) Representative TEM images, c) Particle size distribution histograms and d) XRD patterns of SPIONs. Particle size histograms were plotted after measuring at least 150 particles per sample. Magnetite Standard (Joint Committee on Powder Diffraction Standards – JCPDS card number 89-0691).

indicates a poorer crystallinity in comparison with those obtained at 19.2 s and 27.4 s.

3.2. Effect of micropatterned plates assembly

The results obtained using a staged assembly of plates to separate the nucleation and growth stages, were compared to those on a single microreactor operating either at 180 °C or at 280 °C (Fig. 3-a). An orange-colored solution (similar to the reagent solution injected) resulted after operating the microfluidic system at 180 °C. This solution did not contain any SPIONs or at least, the size was too small to be magnetically separated after the purification steps. The decomposition temperature of iron(III) acetylacetonate is approximately 180 °C [7]; this fact could explain the negligible growth of nanocrystals under those conditions. In fact, this temperature was selected in previous studies to promote the formation of just nuclei [6,7]. On the other hand, a black colloid was obtained after heating the microreactor at 280 °C (Fig. 3-a). TEM analysis evidenced the production of SPIONs with a heterogeneous size distribution, exhibiting a large dispersity (Fig. 3-b, c). XRD spectra confirmed the presence of a pure magnetite phase (Fig. 3-d). The uneven nucleation achieved at 280 °C prevented the segregation between the nuclei formation and growth, i.e., new nuclei were formed while the growth of previously formed nuclei was also taking place. In the solution coexisted large NPs that grew faster than the small NPs formed more recently. These results confirmed the need of separating stages in order to better control the particle size distribution.

Leveraging the versatility of the microreactor designed, the number of micropatterned plates was increased by stacking two plates in each microreactor. The microreactor volume increase exerted the advantages of: 1) Increasing the productivity at fixed t_m value and 2) to explore new reaction conditions (t_m and linear velocity) that were not previously feasible due to microchannel clogging. With high flow rates, the linear velocity is, preventing the microchannel fouling and blockage. This microfluidic configuration with stacked plates successfully ran the SPIONs production for at least 8 h without blockage. The quality of the SPIONs collected was studied along the 8 h of operation time, observing a good reproducibility along operation time. The SPIONs collected at different runs also corroborated that the proposed microsystem was able to assure a good run-to-run reproducibility.

Fig. 4 depicts the TEM images of SPIONs produced with two stacked plates per microreactor. It can be observed that the morphology of resulted SPIONs is similar to those produced with single-plate units. The mean particle size and standard deviation could be considered similar at t_m = 27.4 s whether obtained with 1 or 2 plates, with mean particle sizes of 3.5 ± 0.8 and 3.8 ± 0.8 nm, respectively. However, the analysis of TEM images of SPIONs produced at t_m = 19.2 s resulted in a slightly broader particle size distribution when 2 plates (3.9 ± 0.9 nm) where used instead of 1 (3.4 ± 0.6 nm), Fig. 4. This difference could be the result of the increase of the axial dispersion coefficient as the flow rate is increased, broadening the reactor residence time distribution [24,25]. This is the main reason why droplet-flow reactors, where velocity dispersion is eliminated, have been considered to produce

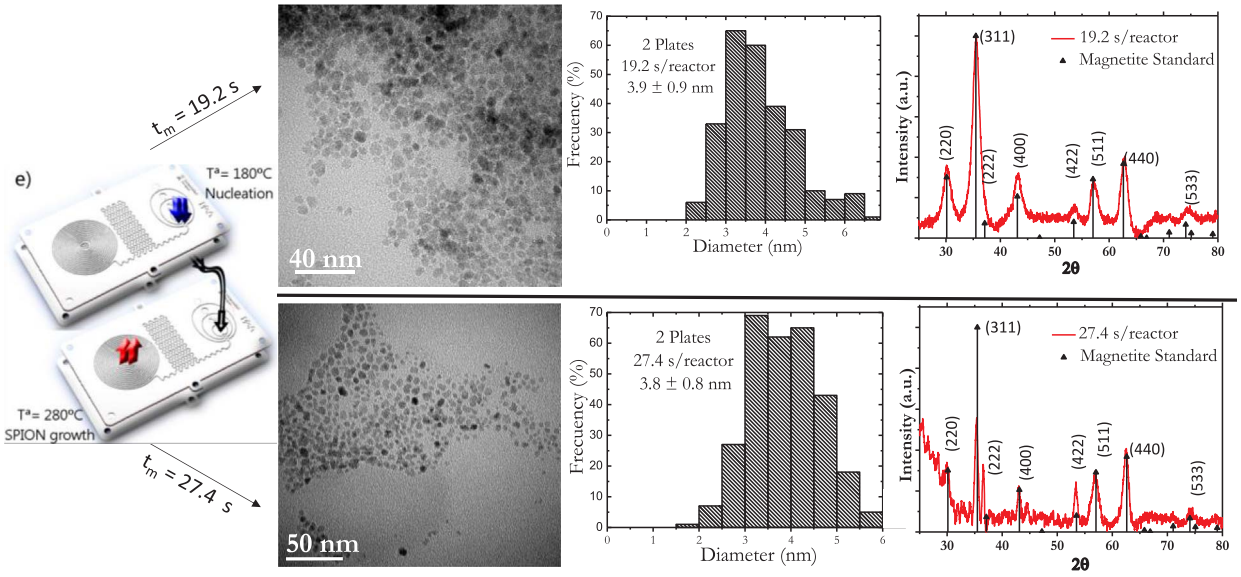

Fig. 4. Production of SPIONs with two microreactors assembled in series with two stacked plates at t_m = 19.2 s and 27.4 s: 1) Nucleation at 180 °C and 2) Growth at 280 °C. Scheme of stream distribution; Representative TEM images, Particle size distribution histograms and XRD patterns of SPIONs. Particle size histograms were plotted after measuring at least 150 particles per sample. Magnetite Standard (Joint Committee on Powder Diffraction Standards – JCPDS card number 89-0691).

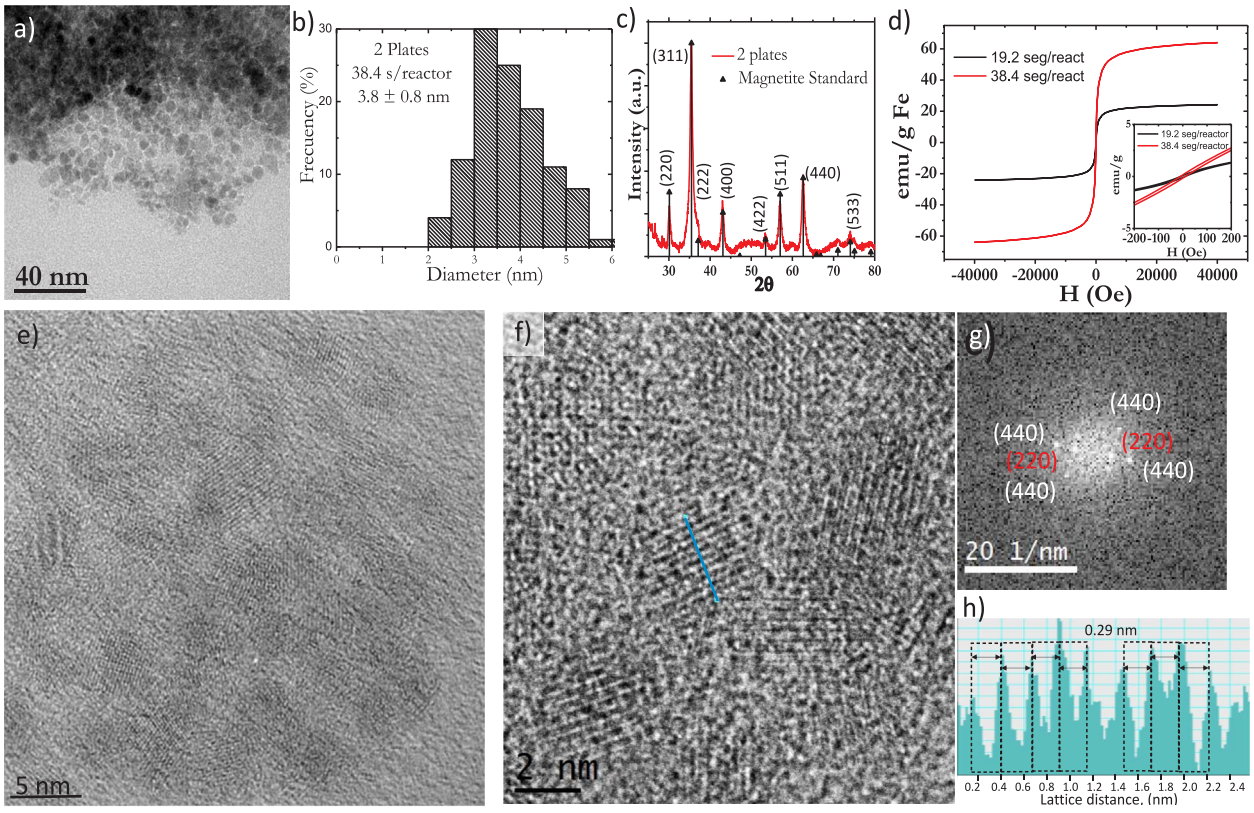

Fig. 5. SPIONs produced with two microreactors assembled in series and stacking two plates at t_m = 38.4 s: 1) Nucleation at 180 °C and 2) Growth at 280 °C. a) TEM image of representative SPIONs. b) Particle size distribution histogram. Particle size histograms were plotted after measuring at least 150 particles per sample. c) XRD pattern. Magnetite Standard (Joint Committee on Powder Diffraction Standards – JCPDS card number 89-0691). d) Magnetization curves of SPIONS produced at t_m = 19.2 and 38.4 s measured at 37 °C. e) and f) HRTEM images to show the crystallinity of SPIONs. g) FFT spectra image of a single SPION. h) Measured lattice spacing from the profile blue marked in f).

SPIONs [14,15,18] as well as in the synthesis of other nanomaterials [11,25]. However, droplet-flow reactors involve the formation of the NPs in aqueous droplets within an oil-based carrier phase. The oil phase and the surfactants used to control droplet size must be subsequently separated from the formed nanoparticles [19], which is not always possible, in addition to the economic cost of separation.

The microfluidic system composed of two microreactors assembled in series with two stacked plates was selected to investigate the properties of the SPIONs produced at t_m higher than 27.4 s. Fig. 5-a depicts the TEM images and particle size distribution of SPIONs produce with t_m of 38.4 s (Flow rate = 500 µL/min). The production of SPIONs at these conditions was stable and no microchannel blockage was observed. Spiral microchannels exhibit transverse Dean flows due to the centrifugal forces [26]. These centrifugal effects are enhanced at high values of Re number (Re > 100) [27] and induce the formation of counter-rotating vortices that promote the mixing and reduce the possibility of aggregate sedimentation, and then microchannel blockage.

Considering that the Re value was increased up to 150 by stacking two plates in the microreactor, it can be argued that both a flow rate larger than 500 µL/min and two plates are required to enable a continuous production of SPIONS with t_m > 27.4 s. However, an increase of t_m above 38.4 s also resulted in the microfluidic channels blockage and therefore an increase in the number of stacked plates together with larger flow rates would be required to avoid the microchannel blockage. The mean particle size achieved with t_m = 38.4 s, 3.8 ± 0.8 nm, is the same as that obtained at t_m of 27.4 s (Fig. 5-b). The mean nanoparticle size was comparable to that observed by Simmons et al. (3.6 ± 1 nm) [19], Frenz et al. (4.0 ± 1 nm) [14] and Kumar et al. (3.6 ± 0.8 nm) [15] and improved the size distribution yielded in a batch – type reactor (5.0 ± 2 nm) [7]. XRD spectra also confirmed the presence of pure magnetite nanocrystals with a preferential growth of (311) and (440) crystallographic planes (Fig. 5-c). High resolution microscopy revealed that SPIONs produced with a t_m = 38.4 s are single crystals with a high crystallinity (Fig. 5e and f). Interplanar spacing could be directly determined from the images by measuring the lattice fringes, and it was approximately 0.29 nm, which corresponds to the (220) planes in the spinel-structured magnetite [28]. On the other hand, Fast Fourier Transformation (FFT) was also performed on the HRTEM images of single particles. The FFT spectra image confirmed the presence of (220) and (440) crystallographic planes. The lattice parameter *a* (8.36 Å) and interplanar spacing d_{hkl} (2.96 Å), determined by Braggs law from the position of the (220) peak by XRD diffraction, are in complete agreement with the spinel crystal structure of bulk Fe_3O_4 (8.39 Å) and the interplanar spacing measured by HRTEM, respectively.

On the other hand, the magnetization values showed that the particles prepared at the two different t_m = 19.2 and 38.4 s (Fig. 5-d) present superparamagnetic behavior with no coercivity or remanent magnetization up to 4 Tesla (Fig. 5-d-inset). The resulting nanoparticles yielded overall magnetic moments lower than those measured for pure magnetite samples (i.e., 92 emu/g) which is attributed to the increased disorder at the particle surfaces as the particle size decreases [29]. The particles obtained with a shorter residence time (19.2 s) produced a magnetic moment at 4 Tesla and 37 °C of only 24 emu/g Fe whereas the particles obtained with t_m = 38.4 s showed a magnetic moment at the same conditions of 64 emu/g Fe. This can be attributed to a reduced crystallinity for the nanoparticles obtained at shorter residence times in agreement with the previous literature [30]. This was confirmed by comparing the full-width at half-maximum (FWHM) of the (311) diffraction plane for both materials (results not shown), corroborating broader peaks for the particles obtained at shorter residence time (19.2 s). The saturation magnetization achieved with t_m = 38.4 s

compares favorably to typical values of 50–70 emu/g reported elsewhere in the literature for SPIONs obtained by thermal decomposition in batch type reactors [6,7].

The synthesis yield was determined by UV–VIS spectroscopy analyzing the 350 nm band corresponding to acetylacetonate absorbance [7]. As could be expected, the lowest yield was achieved at the smallest t_d and vice versa, resulting a yield of 73.1, 80.6 and 86.5% at t_m values of 19.2, 27.4 and 38.4 s, respectively. In terms of productivity, these findings implied that the SPIONs production was 0.7 mg/min, 0.5 mg/min and 0.3 mg/min at t_m values of 19.2, 27.4 and 38.4, respectively. This productivity is 50% to 250% higher than that achieved in a comparable batch process previously developed in our laboratory (0.2 mg/min) [7], taking into account: 1) the time required for heating the reagents (15 °C/min nucleation step and 5 °C/min growth stage), 2) reaction time and cooling the SPIONs, 3) reactor volume, 30 mL. It was not possible to compare the productivity of our microreactor against publications from other laboratories because the synthesis yield was not reported in the literature. However, we can compare the residence time required to crystallize SPIONs and the reagents inlet flow used: 1) Simmons et al. used a short residence time but with a low productivity due to the small flow rate (t_m = 12 s and 20 μL/min) [19], 2) Abou-Hassan et al. used a t_m = 16 min and 136 μL/min [31] and Kumar et al. used a t_m = 10.5 min and 200 μL/min [15]. It can be inferred from these data that our microreactor design not only outperforms batch reactors, but also the previous microreactors used for magnetic NPs production, giving a high productivity of monodisperse of SPIONs with a pure and crystalline magnetite phase.

4. Conclusions

SPIONs have been synthesized for the first time in a continuous flow using a high temperature decomposition method. This method enables the dispersion in water of produced SPIONs, as well as eases their use in biomedical applications because TEG is an organic solvent with reduced toxicity. In spite of the high temperatures used (280 °C) the microreactor system can operate for prolonged periods without microchannel plugging. The flexible design allows to increase the production rate by coupling microreactors with stacked plates. In first-stage microreactors, nucleation takes place by decomposition of the Fe precursor at 180 °C. In the second microreactor, the fast growth of nuclei occurred at 280 °C and monodisperse SPIONs were produced with a yield as high as 86.5%, high crystallinity, high purity (100% magnetite) and magnetization, with total residence times of 76 s or lower.

Acknowledgments

This work has been carried out in the framework of the People Program (CIG-Marie Curie Actions, REA grant agreement no. 321642). The authors gratefully acknowledge the financial support of the ERC Consolidator Grant program (ERC-2013-CoG-614715). The Government of Aragon and the European Social Fund are gratefully acknowledged. CIBER-BBN is an initiative funded by the VI National R&D&i Plan 2008–2011 financed by the Instituto de Salud Carlos III with the assistance of the European Regional Development Fund.

References

[1] M. Arruebo, R. Fernández-Pacheco, M.R. Ibarra, J. Santamaría, Magnetic nanoparticles for drug delivery, Nano Today 2 (2007) 22–32.
[2] A.K. Gupta, M. Gupta, Synthesis and surface engineering of iron oxide nanoparticles for biomedical applications, Biomaterials 26 (2005) 3995–4021.
[3] K.D. Bakoglidis, K. Simeonidis, D. Sakellari, G. Stefanou, M. Angelakeris, Size-dependent mechanisms in AC magnetic hyperthermia response of iron-oxide nanoparticles, IEEE Trans. Magn 48 (2012) 1320–1323.
[4] W. Wu, C.Z. Jiang, V.A.L. Roy, Designed synthesis and surface engineering strategies of magnetic iron oxide nanoparticles for biomedical applications, Nanoscale 8 (2016) 19421–19474.
[5] S.-J. Park, S. Kim, S. Lee, Z.G. Khim, K. Char, T. Hyeon, Synthesis and magnetic studies of uniform iron nanorods and nanospheres, J. Am. Chem. Soc. 122 (2000) 8581–8582.
[6] W. Cai, J.Q. Wan, Facile synthesis of superparamagnetic magnetite nanoparticles in liquid polyols, J. Colloid Interface Sci. 305 (2007) 366–370.
[7] N. Miguel-Sancho, O. Bomati-Miguel, A.G. Roca, G. Martinez, M. Arruebo, J. Santamaria, Synthesis of magnetic nanocrystals by thermal decomposition in glycol media: effect of process variables and mechanistic study, Ind. Eng. Chem. Res. 51 (2012) 8348–8357.
[8] N. Miguel-Sancho, O. Bomatí-Miguel, G. Colom, J.P. Salvador, M.P. Marco, J. Santamaría, Development of stable, water-dispersible, and biofunctionalizable superparamagnetic iron oxide nanoparticles, Chem. Mater. 23 (2011) 2795–2802.
[9] V. Sebastian, M. Arruebo, J. Santamaria, Reaction engineering strategies for the production of inorganic nanomaterials, Small 10 (2014) 835–853.
[10] V.S. Cabeza, High and efficient production of nanomaterials by microfluidic reactor approaches, in: X.-Y. Yu (Ed.), Advances in Microfluidics – New Applications in Biology, Energy, and Materials Sciences, InTech, Rijeka, 2016Ch. 17.
[11] S. Marre, K.F. Jensen, Synthesis of micro and nanostructures in microfluidic systems, Chem. Soc. Rev. 39 (2010) 1183–1202.
[12] V. Sebastian, K.F. Jensen, Nanoengineering a library of metallic nanostructures using a single microfluidic reactor, Nanoscale 8 (2016) 15288–15295.
[13] L. Gomez, V. Sebastian, S. Irusta, A. Ibarra, M. Arruebo, J. Santamaria, Scaled-up production of plasmonic nanoparticles using microfluidics: from metal precursors to functionalized and sterilized nanoparticles, Lab. Chip 14 (2014) 325–332.
[14] L. Frenz, A. El Harrak, M. Pauly, S. Begin-Colin, A.D. Griffiths, J.C. Baret, Droplet-based microreactors for the synthesis of magnetic iron oxide nanoparticles, Angew. Chem. Int. Ed. 47 (2008) 6817–6820.
[15] K. Kumar, A.M. Nightingale, S.H. Krishnadasan, N. Kamaly, M. Wylenzinska-Arridge, K. Zeissler, W.R. Branford, E. Ware, A.J. deMello, J.C. deMello, Direct synthesis of dextran-coated superparamagnetic iron oxide nanoparticles in a capillary-based droplet reactor, J. Mater. Chem. 22 (2012) 4704–4708.
[16] A. Abou-Hassan, O. Sandre, S. Neveu, V. Cabuil, Synthesis of goethite by separation of the nucleation and growth processes of ferrihydrite nanoparticles using microfluidics, Angew. Chem. Int. Ed. 48 (2009) 2342–2345.
[17] V.T. Thu, A.N. Mai, L. Tam, H.V. Trung, P.T. Thu, B.Q. Tien, N.T. Thuat, T.D. Lam, Fabrication of PDMS-based microfluidic devices: application for synthesis of magnetic nanoparticles, J. Electron. Mater. 45 (2016) 2576–2581.
[18] A. Larrea, V. Sebastian, A. Ibarra, M. Arruebo, J. Santamaria, Gas slug microfluidics: a unique tool for ultrafast, highly controlled growth of iron oxide nanostructures, Chem. Mater. 27 (2015) 4254–4260.
[19] M. Simmons, C. Wiles, V. Rocher, M.G. Francesconi, P. Watts, The preparation of magnetic iron oxide nanoparticles in microreactors, J. Flow Chem. 3 (2013) 7–10.
[20] V. Sebastian, N. Zaborenko, L. Gu, K.F. Jensen, Microfluidic assisted synthesis of hybrid Au-Pd dumbbell-like nanostructures: sequential addition of reagents and ultrasonic radiation, Cryst. Growth Des. 17 (2017) 2700–2710.
[21] V. Sebastian, C.D. Smith, K.F. Jensen, Shape-controlled continuous synthesis of metal nanostructures, Nanoscale 8 (2016) 7534–7543.
[22] S. Marre, A. Adamo, S. Basak, C. Aymonier, K.F. Jensen, Design and packaging of microreactors for high pressure and high temperature applications, Ind. Eng. Chem. Res. 49 (2010) 11310–11320.
[23] J. Baek, P.M. Allen, M.G. Bawendi, K.F. Jensen, Investigation of indium phosphide nanocrystal synthesis using a high-temperature and high-pressure continuous flow microreactor, Angew. Chem. Int. Ed. 50 (2011) 627–630.
[24] A. Gunther, S.A. Khan, M. Thalmann, F. Trachsel, K.F. Jensen, Transport and reaction in microscale segmented gas-liquid flow, Lab. Chip 4 (2004) 278–286.
[25] V.S. Cabeza, S. Kuhn, A.A. Kulkarni, K.F. Jensen, Size-controlled flow synthesis of gold nanoparticles using a segmented flow microfluidic platform, Langmuir 28 (2012) 7007–7013.
[26] F. Schonfeld, S. Hardt, Simulation of helical flows in microchannels, AICHE J. 50 (2004) 771–778.
[27] A.P. Sudarsan, V.M. Ugaz, Fluid mixing in planar spiral microchannels, Lab. Chip 6 (2006) 74–82.
[28] Q. Wan, L.S. Xie, L. Gao, Z.Y. Wang, X. Nan, H.L. Lei, X.J. Long, Z.Y. Chen, C.Y. He, G. Liu, X. Liu, B.S. Qiu, Self-assembled magnetic theranostic nanoparticles for highly sensitive MRI of minicircle DNA delivery, Nanoscale 5 (2013) 744–752.
[29] X. Huang, Z. Chen, Nickel ferrite on silica nanocomposites prepared by the sol–gel method, J. Magn. Magn. Mater. 280 (2004) 37–43.
[30] Â.L. Andrade, M.A. Valente, J.M.F. Ferreira, J.D. Fabris, Preparation of size-controlled nanoparticles of magnetite, J. Magn. Magn. Mater. 324 (2012) 1753–1757.
[31] A. Abou-Hassan, S. Neveu, V. Dupuis, V. Cabuil, Synthesis of cobalt ferrite nanoparticles in continuous-flow microreactors, RSC Adv. 2 (2012) 11263–11266.